ELSEVIER

Contents lists available at ScienceDirect

## International Journal of Heat and Mass Transfer

journal homepage: www.elsevier.com/locate/ijhmt



# On the influence of tissue anisotropy in numerical modelling of radiofrequency ablation

Romain Fichter <sup>a</sup>, Damijan Miklavčič <sup>b</sup>, Bor Kos <sup>b,\*</sup>

### ARTICLE INFO

### Keywords: Radiofrequency ablation Muscle anisotropy Electrical conductivity Thermal conductivity

### ABSTRACT

Background: The numerical modeling of radiofrequency ablation (RFA) has improved considerably in recent years. Successful modeling requires a detailed understanding of the properties of biological tissue. Due to their anatomical structure, skeletal and cardiac muscles exhibit anisotropic properties that can lead to different conduction of electrical current and heat transfer depending on fiber orientation. We therefore investigated whether tissue anisotropy also has an influence at the relatively high frequencies used in RFA (~500 kHz). Methods: In a time-dependent study, we used the finite element method to model the electrical currents and heat transfer to calculate the temperature distribution in vivo. We investigated the effects of the anisotropic electrical and thermal properties of the muscles on the accuracy of the model. The model was compared with the experimental results and the accuracy of the model was quantitatively evaluated using the Sørensen-Dice coefficient

Results: Despite the relatively high frequency of the alternating electric current used in RFA, the anisotropy of the electrical conductivity of the muscles has a significant effect on the accuracy of the model. The numerical model with an anisotropy ratio of 1.5 achieved the highest average Sørensen-Dice coefficient. However, the anisotropy of the thermal conductivity does not seem to affect the model accuracy (no significant change compared to the model without anisotropy).

### 1. Introduction

Radiofrequency ablation (RFA) is a commonly employed technique for treating cardiac arrhythmias[1]. The aim of catheter ablation in the heart is to destroy arrhythmogenic tissue, or, in the case of atrial fibrillation (AF), the most common cardiac arrhythmia, to electrically isolate the pulmonary veins from the rest of the atrium, by creating a contiguous lesion around the ostium of the veins, as this is where most of the triggers of atrial fibrillation are located [2]. Ablated myocardium does not regenerate, but is instead replaced by fibrotic tissue, which does not conduct action potentials. Although recent rapid adoption of pulsed field ablation is moving the field away from RFA,[3] RFA still represents a considerable fraction of all global procedures, especially in the ventricles. During the years of evolution of RFA technology, various methods and biomarkers were investigated to improve lesion durability and procedural success. These include, for example, electroanatomical mapping, [4] which helps to navigate inside the heart and reliably determine the distances between lesions, and the measurement of contact force, which ensures good contact with the tissue and is also used as a surrogate marker for lesion size [5,6] Interestingly, a recent publication using a temperature-controlled catheter showed no significant dependence of lesion depth on contact force in a thigh skeletal muscle tissue surrogate model [7]. However, a detailed examination of the images obtained in these experiments revealed relatively large variations in lesion width and shape, which we hypothesize to be related to muscle fiber orientation.

One important property of striated muscle tissue is its inherent anisotropy [8,9]. The myocardium exhibits a highly organized fibrous structure [10], leading to directional variations in electrical conductivity. Anisotropy is also present in skeletal muscle, that is used in the thigh model [11]. These anisotropic characteristics affect the electric current and electric field distribution and consequently tissue heating and potentially heat conduction and dissipation in tissue. The temperature distribution is dependent on the heat dissipation and conduction during the RFA treatment, which affects the lesion size, shape, and depth. Myocardium and skeletal muscle have long been known to have

E-mail address: bor.kos@fe.uni-lj.si (B. Kos).

<sup>&</sup>lt;sup>a</sup> Universite Claude Bernard Lyon 1, Polytech Lyon, Villeurbanne, France

<sup>&</sup>lt;sup>b</sup> University of Ljubljana, Faculty of Electrical Engineering, Ljubljana, Slovenia

<sup>\*</sup> Corresponding author.

anisotropic conductivity [8,12–15]. The anisotropy ratio between the longitudinal (along the fibers) and transverse (across the fibers) conductivity is frequency dependent. It is most pronounced at low frequencies (<1 kHz), but with increasing frequency the two conductivities become very similar. This is consistent with the  $\beta$  relaxation region of tissue dielectric properties, during which the cell membranes which present a barrier to low-frequency current become transparent to the current due to capacitive coupling across the thin membrane [16]. Recently, also a small anisotropy in thermal conductivity has been reported in muscle tissue [17].

Recent RFA modelling studies suggested a possible effect of tissue anisotropy on lesion size and shape. Perez et al. have shown a small change in lesion size when considering anisotropic tissue properties [18]. Molinari et al. [19] have used ex vivo myocardium slices harvested from a commercial slaughterhouse and noticed a marked influence of tissue anisotropy on lesion shape, although they do not report the elapsed time between tissue excision and experiments.

With our study, we aim to investigate the role of anisotropic skeletal tissue properties on RFA lesion formation in the thigh muscle model, examining their impact on lesion geometry. We hypothesize that electrical conductivity anisotropy has an important effect on the shape of the lesion. We also hypothesize that thermal conductivity does not, because the cell membrane is too thin to present an effective thermal barrier. We investigated relative contribution of tissue conductivity of tissue electrical and thermal conductivity on RFA by comparing temperature distribution obtained in numerical modeling with experimental in vivo lesion size and shape.

### 2. Material and methods

### 2.1. Numerical model geometry and tissue properties

Numerical modeling was performed using COMSOL Multiphysics (version 6.2, COMSOL AB, Stockholm, Sweden). The muscle was modeled as a cuboid with dimensions of  $20~\rm cm$  in length,  $20~\rm cm$  in width, and  $10~\rm cm$  in height (Fig. 1).

The experimental setup [7] was recreated. The cup with blood perfusion that was placed on the muscle surface was modeled as a cylinder with a radius of 22.5 mm and a height of 85 mm. A numerical representation of the Diamond Temp catheter was made using measurement and drawings of the physical device.

The electrical conductivity of tissue  $\sigma$  was considered to increase by +1.5 % per degree Celsius up to 100 °C [20]. At a baseline temperature of 37 °C, the conductivity of the skeletal muscle was 0.541 S/m , but

when approaching 100 °C it was decreased to  $1.371 \times 10^{-4}$  S/m to account for the tissue desiccation process [21]. Thermal conductivity was set to  $0.531~W\cdot(m\cdot K)^{-1}$  [22]. The properties of swine blood were used to model the blood flow within the cup. The blood was kept at constant body temperature.

### 2.2. Numerical model setup

We performed a time-domain heat transfer simulation to determine the initial temperature values in the outermost layers of the muscle that were subjected to convective cooling by air exposure during the experiment. The air exposure results from the experimental protocol in which the thigh muscle was surgically opened and, after a certain delay, the cylindrical cup was positioned on its surface to maintain blood perfusion around the catheter. These results were validated using the temperature measurements of the thermocouples at the catheter tip, which were measured before the start of ablation.

To take this into account, a transient heat transfer model was solved over the exposed muscle area. The relevant heat transfer equation with convective transport was:

$$\rho C_p \boldsymbol{u} \cdot \nabla T + \nabla \cdot \boldsymbol{q} = Q_{electrical}$$

Where  $\rho$  is the tissue density,  $C_p$  is the specific heat capacity, u is the velocity field (nonzero in perfused regions), T is the temperature, q is the conductive heat flux, Q is the volumetric heat source (Joule heating, during ablation).

The conductive heat flux was defined according to Fourier's law:

$$q = -k\nabla T$$

with k the thermal conductivity of the tissue.

The ablation itself was modeled using a time-domain simulation in which the quasi-static calculation of the electric fields in the tissue and the resulting ohmic heating and heat transfer were coupled. Although the catheter used in the experiments is temperature-controlled and the electrical power is reduced as soon as the target temperature measured by the thermocouples on the catheter is reached, we used a constant power of 50 W in the simulations, as the target temperature of 60  $^{\circ}\text{C}$  was not reached in the majority of the experiments. The ablation electrodes were set up as a terminal boundary condition, and the indifferent electrode positioned at the bottom of the cuboid. The frequency was 500 kHz. In a separate study, laminar flow was modeled in the blood perfusion chamber to contribute to heat advection due to blood and saline perfusion.

The electric potential distribution was calculated by solving the

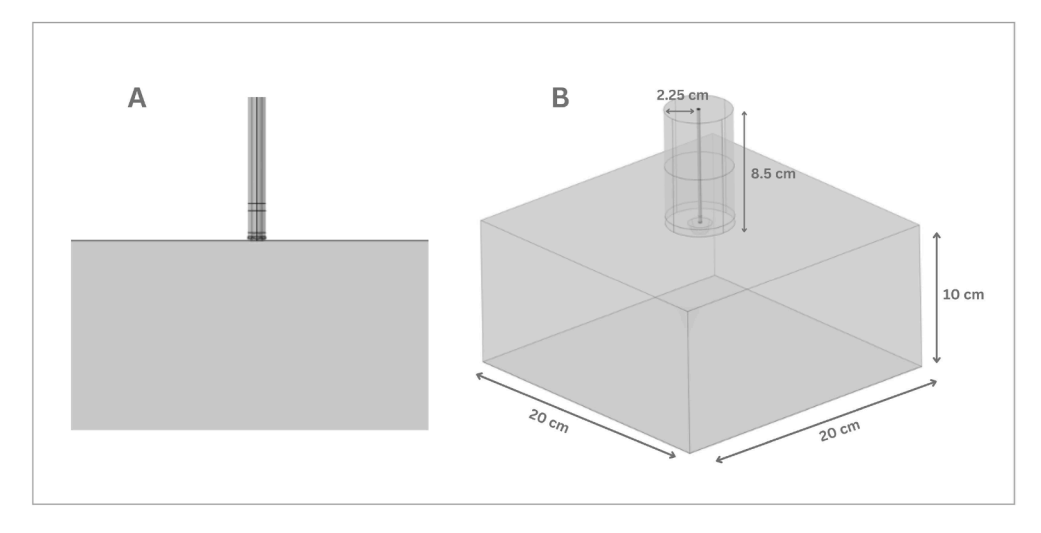


Fig. 1. (A) Side view cross-section of the computational geometry without the cylindrical domain representing the blood flow. (B) Geometry of the computational domain implemented in COMSOL Multiphysics®, showing the main structural components and associated dimensions used in the numerical model.

following coupled equations across the entire computational domain:

$$abla \cdot oldsymbol{J} = Q_{(j.V)}, oldsymbol{J} = \sigma oldsymbol{E} + oldsymbol{J}_e \ oldsymbol{E} = -
abla V$$

where J is the current density,  $\sigma$  the electrical conductivity, E the electric field, V the electric potential, and  $J_e$  the externally applied current source. The Joule heating term represents the volumetric heat source due to electrical current.

A terminal boundary condition was applied to the ablation electrode, and an electric ground was set at the indifferent electrode located at the bottom of the cuboidal domain. The frequency was 500 kHz. Electrical insulation was applied to all other external boundaries, using the Neumann condition:

$$n \cdot \mathbf{J} = 0$$

to ensure no current leakage across the outer surfaces.

The initial blood temperature was obtained by using catheter tip sensor measurements ( $\sim$ 35 °C). A laminar saline solution flow rate of 8 ml/min was established within the catheter. While the blood flow within the cylindrical cup was set at 12 cm/s at the inlet of the cup. The blood inlet was defined on a surface corresponding to half of the base of the cylindrical cup. The cylinder was longitudinally divided into two equal halves, with a constant blood flow velocity of 12 cm/s imposed at the inlet surface of one half, assuming flow exited through the opposite outlet surface.

To replicate the experimental setup, the cylindrical domain was longitudinally divided into two equal halves. A constant velocity of 12 cm/s was imposed on the inlet surface of one half of the cylinder base, while the outlet was defined on the opposite surface of the other half, enabling continuous flow through the volume.

The fluid flow was assumed laminar and incompressible, governed by the Navier–Stokes and continuity equations, which were solved over the fluid domain as follows:

$$\begin{aligned} (\rho(\boldsymbol{u}{\cdot}\nabla)\boldsymbol{u} &= \nabla{\cdot}[-p2\mathbf{I} + \mathbf{K}] \\ \rho\nabla{\cdot}\boldsymbol{u} &= 0 \end{aligned}$$

Where  $\rho$  is the fluid density, u is the velocity vector, p is the pressure, I is the identity tensor, K represents the viscous stress tensor.

The computational domain was discretized using the finite element method in COMSOL Multiphysics®. An unstructured mesh was generated, with localized refinement around the electrode–tissue interface and within the muscle domain to ensure higher resolution in regions exhibiting steep thermal and electrical gradients. The final mesh consisted of 1130,756 domain elements.

This mesh configuration was chosen after a convergence analysis to ensure that further refinement did not significantly alter the temperature distribution or lesion dimensions. The refined region under the catheter was essential to accurately capture the localized heat transfer mechanisms critical to lesion formation during RFA.

To ensure that the numerical solution is independent of the mesh resolution, a mesh independence study was performed. Different grid densities were generated with local refinement around the ablation catheter, where steep thermal and flow gradients are expected. Two refinement levels were tested in the catheter region (fine and extra-fine), while in the remaining domain medium and fine grids were employed. The key monitored quantities were the maximum tissue temperature and the average heat flux at the catheter–tissue interface. The results show that no significant variation was observed between the fine and extra-fine meshes around the catheter, with differences below 0.2 % in both maximum temperature and heat flux. Therefore, the fine mesh was considered sufficient to accurately capture the relevant physics while reducing computational cost. This mesh configuration was adopted for all subsequent simulations.

### 2.3. Experimental image processing and analysis

We used a previously obtained dataset of images depicting experimental lesions induced by radiofrequency ablation (RFA) on swine thigh muscle stained with TTC dye. This dataset comprised approximately 400 lesions with temperature-controlled power-limited ablation times of 5 s, 10 s, and 15 s was provided by Medtronic [7].

ImageJ software was used for image processing, with which the lesions could be isolated and measured. The spatial scale was calibrated using the ruler reference from the photographs. An optimal thresholding procedure was then applied, adjusting the hue, saturation and brightness parameters to selectively identify lesion pixels. Given the variability of image features, manual adjustments were required on a caseby-case basis to refine the thresholding process and ensure accurate segmentation of lesions. To ensure consistency of analysis, the experimental binary lesion images were standardized in size using a predefined scale. An image section of 10 mm  $\times$  10 mm was chosen to capture the largest lesions while avoiding unnecessary enlargement of the image dimensions. To correct for the deviations that occurred during sample preparation and imaging, the images of the binary lesions were rotated to compensate for the tilt caused by the sectioning and imaging angles. In addition, all images were aligned so that the horizontal area corresponding to the catheter placement was centered within the frame.

To enable a direct comparison between the experimental and theoretical results, it was necessary to extract data from the computational model in an appropriate format. Using MATLAB, the time-dependent variation of temperature within the modeled muscle during RFA was obtained. A temperature threshold of 50  $^{\circ}\mathrm{C}$  was applied to determine lesion size across different ablation durations. The computational models were segmented into three configurations, corresponding to the experimental ablation times of 5 s, 10 s, and 15 s.

We evaluated several models of cell death to identify the most appropriate fit for the experimental data. These included a classical first-order Arrhenius model [23], a three-step Arrhenius model [24], and various fixed temperature threshold models. Each approach yielded different outcomes in terms of lesion prediction accuracy. Among them, the best overall agreement with experimental observations was the one using a temperature threshold of 50  $^{\circ}$ C [25,26], which was therefore adopted as the reference model in this study.

### 2.4. Estimation of fiber orientation

One of the limitations of the experimental raw images was the lack of important information about the alignment of the muscle fibers. Identifying whether the lesion cross-section represents fibers that are aligned with the cut or oriented at an angle was not possible without additional experimental analysis, such as microscopic examination to determine the primary fiber direction.

To overcome this challenge, a comparison algorithm was implemented to retrospectively estimate the most probable fiber orientation. Within the model, four predefined planes were selected, each rotated by a different angle relative to the muscle fibers. The first plane represented a normal cross-section, modeling a cut perpendicular to the fiber orientation, ie.  $90^{\circ}$  Three other planes were considered at an angle of  $30^{\circ}$  and  $60^{\circ}$  relative to the fiber direction and one plane parallel to the fibers ie.  $0^{\circ}$  The accuracy of each model plane was determined by comparing each of the simulated lesion shape with the experimental image. The configuration with the highest accuracy was selected as the best matching fiber orientation. The Sørensen-Dice coeeficient was used to compare the experimental results and the numerical model.

### 3. Results

Anisotropy of electrical current flow, electric field distribution, and current tissue heating were implemented with different anisotropy values (20 %, 50 % and 70 %). Implementing 20 % anisotropy in

electrical conductivity implies that conductivity is reduced by 20 % in all directions orthogonal to the muscle fiber orientation, relative to the conductivity along the fiber axis. When a 20 % value was assessed, the median value of accuracy was not significantly different than in the reference model (p < 0.05) but still, a small increase in accuracy was observed. For higher values of anisotropy, results were significantly better with a median value of accuracy that increases up to 0.80 and 0.78 for 50 % and 70 % of anisotropy respectively (Table 1).

Fig. 2 Comparative analysis of lesion overlap between two computational models incorporating different degrees of anisotropy in electrical conductivity. The first model assumes isotropic electrical conductivity (0 % anisotropy), (Fig. 2B and E) while the second accounts for a high degree of anisotropy (70 %) (Fig. 2C and F). The first row depicts a lesion where the impact of anisotropy on lesion morphology is significant (Fig. 2A), whereas the second row illustrates a lesion where anisotropy appears to have a lesser influence on the lesion shape (Fig. 2D). The results indicate that incorporating anisotropic conductivity into the model alters lesion shape, primarily by increasing lesion width along the direction of the fibers. This effect can be attributed to enhanced electrical current propagation along the myocardial fiber direction, leading to a more extended lesion shape.

Fig. 3 shows boxplots of Sørensen-Dice coefficients scores for different ablation durations and different degrees of anisotropy applied to different physical properties. Panels A, B and C correspond to ablation times of 5 s, 10 s, and 15 s, respectively. In each case, the Sørensen-Dice coefficient is shown as a function of the percentage of anisotropy for thermal conductivity (purple), electrical conductivity (orange), and their combination (blue). The yellow field corresponds to the reference model without anisotropy. Panel D shows a consolidated comparison of the influence of the anisotropy of electrical conductivity across all ablation durations. The statistical analysis performed for the four groups shown in panel D revealed a significant overall difference between the groups (p < 0.025, one-way ANOVA).

Post hoc analysis revealed that statistically significant differences (p < 0.01) were concentrated around the 50 % anisotropy model. Specifically, significant differences were observed between the 20 % and 50 % anisotropy models, as well as between the isotropic model (0 %) and the 50 % anisotropy model. In contrast, no significant difference was found between the 0 % and 20 % models, nor between the 50 % and 70 % anisotropy models (p > 0.025).

In Fig. 3, panel A (5 s ablation), the highest Sørensen-Dice coefficient values are observed for models with 70 % anisotropy in electrical conductivity and in the combined anisotropic case, indicating improved prediction accuracy under these conditions. Conversely, anisotropy applied only to thermal conductivity does not appear to significantly

Table 1
Median Sørensen-Dice coefficient obtained for different anisotropy configurations applied to thermal conductivity, electrical conductivity, and their combination. The third row ("Isotropic") corresponds to the baseline model, in which no anisotropy was considered. Each value corresponds to the median model accuracy across all evaluated samples, for a given percentage of anisotropy.

Ablation Time	5s	10s	15s	Total
Sample size	130	165	141	436
Isotropic	0.56	0.69	0.73	0.67
Electrical conductivity anisotropy				
20 %	0.60	0.71	0.75	0.69
50 %	0.70	0.81	0.81	0.80
70 %	0.71	0.80	0.80	0.78
Thermal conductivity anisotropy				
20 %	0.57	0.70	0.74	0.68
50 %	0.59	0.73	0.76	0.71
70 %	0.61	0.76	0.78	0.74
Electrical & Thermal conductivity anisotropy				
20 %	0.60	0.72	0.76	0.71
50 %	0.69	0.80	0.80	0.79
70 %	0.73	0.79	0.76	0.78

affect model performance. Similar trends are observed in panels B and C (10 s and 15 s ablation), where optimal agreement between model and experiment is achieved for anisotropy levels between 50 % and 70 % of the electrical conductivity. Finally, panel D confirms that the best overall agreement between predicted and experimental lesions is consistently achieved when the anisotropy of the electrical conductivity is considered in the range of 50–70 %, independent of the ablation duration.

### 4. Discussion

All results show that a higher degree of anisotropy in the electrical conductivity leads to a better agreement between the model predictions and the experimental data. As summarized in Table 1, the lowest model accuracy is observed for samples subjected to a 5-second ablation, with the reference (isotropic) model yielding a mean Sørensen-Dice coefficient of 0.5624. In contrast, the highest values for this ablation duration are obtained when a 70 % anisotropy is applied to the electrical conductivity (0.7141) and to the electrical and thermal conductivity (0.7330). Similar trends are observed for the 10- and 15-second ablations: the best results are consistently obtained with an anisotropy applied to electrical conductivity. The overall performance, as shown in the total row of Table 1, confirms that the best prediction accuracy is achieved with a 50 % anisotropy of electrical conductivity (mean Sørensen-Dice coefficient of 0.8006). Comparable values are obtained for a combined anisotropy of electrical and thermal conductivity at 50 % (0.7844) and 70 % (0.7860). In contrast, anisotropy applied only to thermal conductivity leads to less significant improvements, with Sørensen-Dice coefficient of 0.6836, 0.7088 and 0.7388 for anisotropy levels of 20 %, 50 % and 70 % respectively. Compared to the reference model (mean Sørensen-Dice coefficient value of 0.6741), these values show that the anisotropy of thermal conductivity alone does not significantly improve the predictive performance of the model, especially when compared to the effects of the anisotropy of electrical conductivity.

The presence of outliers in Fig. 3, represented by circles, is particularly noticeable in some test samples, which are characterized by abnormally small lesion sizes. These deviations may indicate suboptimal catheter–tissue contact during the ablation procedure, resulting in limited energy delivery and suboptimal lesion formation.

The results obtained in this study support the hypothesis raised by previous works regarding the influence of skeletal muscle anisotropy on lesion development in RFA [18,19]. The observed preferential propagation of electrical current along the muscle fiber direction suggests that anisotropic properties may significantly affect both lesion size and shape prediction during radiofrequency ablation (RFA) procedures.

The study has several limitations. The direction of fibers was not extracted from experimental images but was deduced by matching the best fitting simulated lesion on the experimental lesion. The external cooling by circulating blood in the thigh prep model was not modelled to a high fidelity, as the exact geometry of the experimental apparatus was not available.

### 5. Conclusions

The results of our study show that considering electrical conductivity anisotropy improves the agreement between simulated and experimental RFA size and shape of lesions when a 50 °C isotherm is assumed as the ablated volume. Although the ratio of tissue anisotropy at high frequencies (500 kHz for RFA) is smaller than at lower frequencies, sufficient anisotropy remains to justify its inclusion in the numerical evaluation of radiofrequency ablation. The anisotropy of thermal conductivity, on the other hand, does not improve the agreement between experiments and simulations.

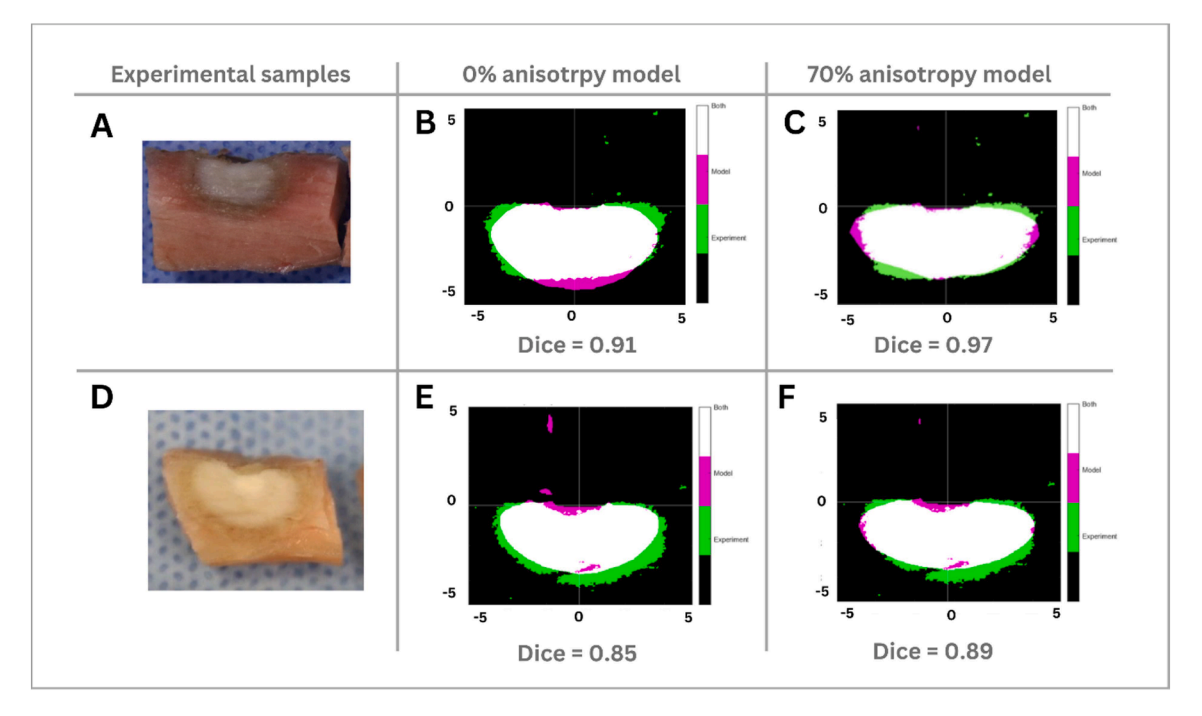
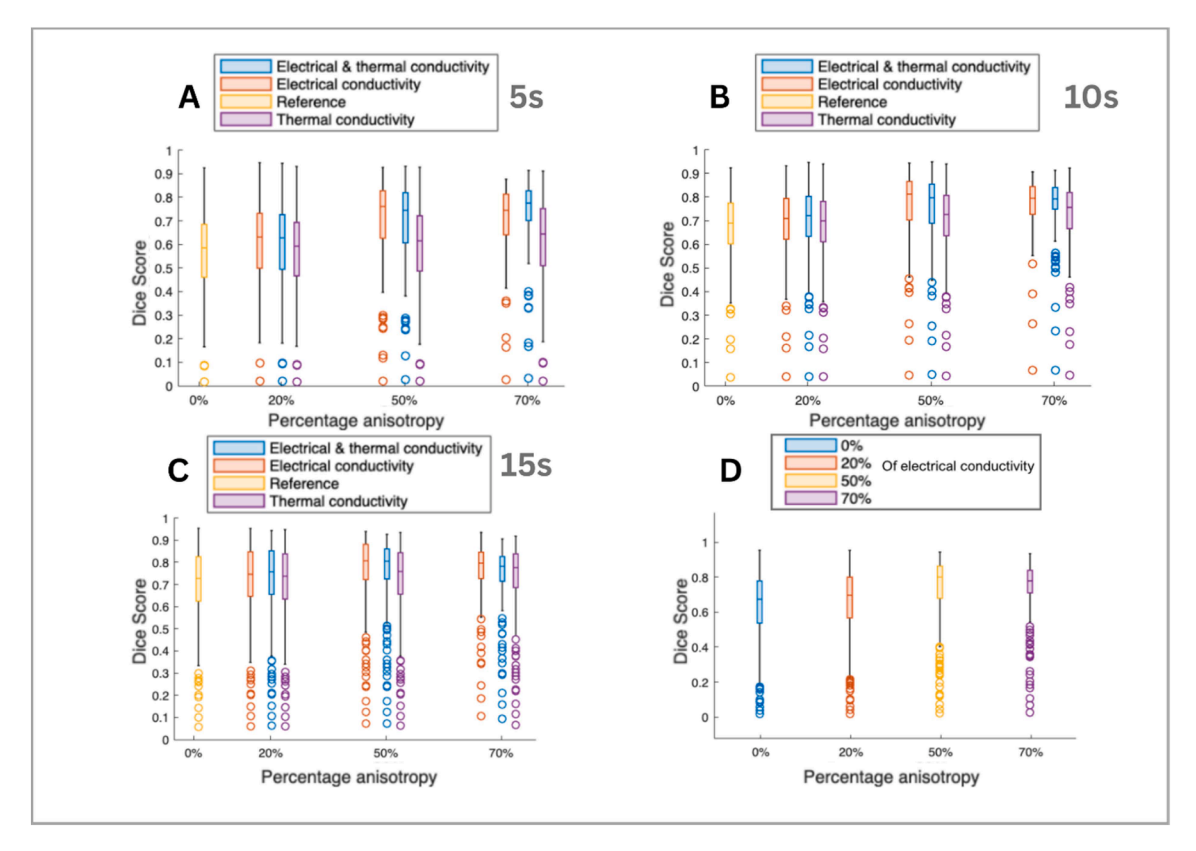


Fig. 2. Representative comparison between experimental lesions and model predictions, with and without anisotropy. (A) Experimental lesion. (B) Superposition of the lesion shown in (A) with the model prediction without anisotropy. The experimental lesion is shown in green, the model output is pink, and the overlapping region is white. (C) Superposition of the lesion shown in (A) with the model prediction incorporating 70 % anisotropy on electrical conductivity, oriented along the principal direction of anisotropy. (D) Experimental lesion for a case exhibiting low anisotropy along the fiber direction. (E) Superposition of the lesion shown in (D) with the model prediction without anisotropy. (F) Superposition of the lesion shown in (D) with the model prediction including 70 % anisotropy.



**Fig. 3.** Sørensen-Dice coefficient similarity coefficient as a function of the anisotropy percentage for varying ablation durations. **A:** Ablation time of 5 s: anisotropy is evaluated across different physical parameters and grouped according to anisotropy percentage. **B:** Ablation time of 10 s: anisotropy evaluated across different physical parameters and grouped according to anisotropy percentage. **C:** Ablation time of 15 s: anisotropy evaluated across different physical parameters and grouped according to anisotropy percentage. **D:** Comparison of anisotropy effects considering electrical conductivity only, for ablation durations of 5 s, 10 s, and 15 s.

### CRediT authorship contribution statement

Romain Fichter: Writing – review & editing, Writing – original draft, Visualization, Methodology, Investigation, Formal analysis. Damijan Miklavčič: Writing – review & editing, Writing – original draft, Funding acquisition, Conceptualization. Bor Kos: Writing – review & editing, Writing – original draft, Supervision, Conceptualization.

### Declaration of competing interest

The authors declare the following financial interests/personal relationships which may be considered as potential competing interests: Damijan Miklavcic reports financial support and article publishing charges were provided by Slovenian Research and Innovation Agency. Bor Kos reports a relationship with Medtronic Inc that includes: consulting or advisory. Damijan Miklavcic reports a relationship with Medtronic Inc that includes: consulting or advisory and funding grants. Damijan Miklavcic reports a relationship with Inomagen Therapeutics that includes: consulting or advisory. Damijan Miklavcic reports a relationship with Boston Scientific Corporation that includes: speaking and lecture fees. If there are other authors, they declare that they have no known competing financial interests or personal relationships that could have appeared to influence the work reported in this paper.

### Acknowledgements

The authors would like to acknowledge Peter Lombergar for assistance with numerical modeling using COMSOL Multiphysics.

#### Data availability

Data will be made available on request.

### References

- [1] T.J. Buist, D.P. Zipes, A. Elvan, Atrial fibrillation ablation strategies and technologies: past, present, and future, Clin. Res. Cardiol. 110 (2021) 775–788, https://doi.org/10.1007/s00392-020-01751-5.
- [2] M. Haïssaguerre, P. Jaïs, D.C. Shah, A. Takahashi, M. Hocini, G. Quiniou, S. Garrigue, A. Le Mouroux, P. Le Métayer, J. Clémenty, Spontaneous Initiation of Atrial Fibrillation by Ectopic Beats Originating in the Pulmonary Veins, N. Engl. J. Med. 339 (1998) 659–666, https://doi.org/10.1056/NEJM199809033391003.
- [3] K.-R.J. Chun, D. Miklavčič, K. Vlachos, S. Bordignon, D. Scherr, P. Jais, B. Schmidt, State-of-the-art pulsed field ablation for cardiac arrhythmias: ongoing evolution and future perspective, Europace 26 (2024) euae134, https://doi.org/10.1093/ arrapse/cyus-124
- [4] Sanjiv M. Narayan, Roy M. John, Advanced Electroanatomic Mapping: current and Emerging Approaches, Curr. Treat. Options. Cardiovasc. Med. 26 (4) (2024) 69–91, https://doi.org/10.1007/s11936-024-01034-6.
- [5] Moloy Das, Jonathan J. Loveday, Gareth J. Wynn, et al., Ablation Index, a Novel Marker of Ablation Lesion Quality: prediction of Pulmonary Vein Reconnection at Repeat Electrophysiology Study and Regional Differences in Target Values, Europace (2016) euw105, https://doi.org/10.1093/europace/euw105. May 31.
- [6] Petr Neuzil, Vivek Y. Reddy, Josef Kautzner, et al., Electrical Reconnection After Pulmonary Vein Isolation Is Contingent on Contact Force During Initial Treatment: results From the EFFICAS I Study, Circ.: Arrhythmia Electrophysiol. 6 (2) (2013) 327–333, https://doi.org/10.1161/CIRCEP.113.000374.

- [7] Atul Verma, Megan M. Schmidt, Jean-Pierre Lalonde, David A. Ramirez, Michael K. Getman, Assessing the Relationship of Applied Force and Ablation Duration on Lesion Size Using a Diamond Tip Catheter Ablation System, Circ.: Arrhythmia Electrophysiol. 14 (7) (2021), https://doi.org/10.1161/CIRCEP.120.009541.
- [8] B.R. Epstein, K.R. Foster, Anisotropy in the Dielectric Properties of Skeletal Muscle, Med. Biol. Eng. Comput. 21 (1983) 51–55.
- [9] Rok Šmerc, Marko Stručić, Matej Kranjc, Igor Serša, Damijan Miklavčič, Samo Mahnič-Kalamiza, Electrical Pathways Through the Intricate Network of Skeletal Muscle Fibres: insights From MRI-Validated Numerical Modelling, IEEE Trans. Biomed. Eng. (2025) 1–11, https://doi.org/10.1109/TBME.2025.3572353.
- [10] Kevin L. Sack, Eric Aliotta, Daniel B. Ennis, et al., Construction and Validation of Subject-Specific Biventricular Finite-Element Models of Healthy and Failing Swine Hearts From High-Resolution DT-MRI, Front. Physiol. 9 (May) (2018) 539, https://doi.org/10.3389/fphys.2018.00539.
- [11] Rok Šmerc, David A. Ramirez, Samo Mahnič-Kalamiza, et al., A Multiscale Computational Model of Skeletal Muscle Electroporation Validated Using In Situ Porcine Experiments, IEEE Trans. Biomed. Eng. 70 (6) (2023) 1826–1837, https://doi.org/10.1109/TBME.2022.3229560.
- [12] Stanley Rush, J.A. Abildskov, Richard Mcfee, Resistivity of Body Tissues at Low Frequencies, Circ. Res. 12 (1) (1963) 40–50, https://doi.org/10.1161/01. RES.12.1.40.
- [13] P. Steendijk, E.T. Velde, J. Baan, Dependence of Anisotropic Myocardial Electrical Resistivity on Cardiac Phase and Excitation Frequency, Basic Res. Cardiol. 89 (5) (1994) 411–426, https://doi.org/10.1007/BF00788279.
- [14] S. Gabriel, R.W. Lau, C. Gabriel, The Dielectric Properties of Biological Tissues: II. Measurements in the Frequency Range 10 Hz to 20 GHz, Phys. Med. Biol. 41 (11) (1996) 2251–2269.
- [15] C. Gabriel, A. Peyman, E.H. Grant, Electrical Conductivity of Tissue at Frequencies below 1 MHz, Phys. Med. Biol. 54 (16) (2009) 4863–4878, https://doi.org/ 10.1088/0031-9155/54/16/002.
- [16] K.R. Foster, H.P. Schwan, Dielectric Properties of Tissues and Biological Materials: a Critical Review, Crit. Rev. Biomed. Eng. 17 (1) (1989) 25–104.
- [17] Kai Yue, Liang Cheng, Lina Yang, Bitao Jin, Xinxin Zhang, Thermal Conductivity Measurement of Anisotropic Biological Tissue In Vitro, Int. J. Thermophys. 38 (6) (2017) 92, https://doi.org/10.1007/s10765-017-2214-x.
- [18] Juan J. Pérez, Enrique Berjano, Ana González-Suárez, In-Silico Modeling to Compare Radiofrequency-Induced Thermal Lesions Created on Myocardium and Thigh Muscle, Bioengineering 9 (7) (2022) 329, https://doi.org/10.3390/ bioengineering9070329.
- [19] Leonardo Molinari, Martina Zaltieri, Carlo Massaroni, Simonetta Filippi, Alessio Gizzi, Emiliano Schena, Multiscale and Multiphysics Modeling of Anisotropic Cardiac RFCA: experimental-Based Model Calibration via Multi-Point Temperature Measurements, Front. Physiol. 13 (April) (2022) 845896, https://doi. org/10.3389/fphys.2022.845896.
- [20] David Schutt, Enrique J. Berjano, Dieter Haemmerich, Effect of Electrode Thermal Conductivity in Cardiac Radiofrequency Catheter Ablation: a Computational Modeling Study, Int. J. Hyperth. 25 (2) (2009) 99–107, https://doi.org/10.1080/ 02656730802563051
- [21] D. Haemmerich, L. Chachati, A.S. Wright, D.M. Mahvi, F.T. Lee, J.G. Webster, Hepatic Radiofrequency Ablation with Internally Cooled Probes: effect of Coolant Temperature on Lesion Size, IEEE Trans. Biomed. Eng. 50 (4) (2003) 493–500, https://doi.org/10.1109/TBME.2003.809488.
- [22] Enrique J. Berjano, Theoretical Modeling for Radiofrequencyablation: state-of-the-Art and Challenges for the Future, Biomed. Eng. Online 5 (1) (2006) 24, https://doi.org/10.1186/1475-925X-5-24.
- [23] W.C. Dewey, Arrhenius Relationships from the Molecule and Cell to the Clinic, Int. J. Hyperth. 25 (1) (2009) 3–20, https://doi.org/10.1080/02656730902747919.
- [24] Argyrios Petras, Massimiliano Leoni, Jose M Guerra, Luca Gerardo-Giorda, Calibration of a Three-State Cell Death Model for Cardiomyocytes and Its Application in Radiofrequency Ablation, Physiol. Meas. 44 (6) (2023) 065003, https://doi.org/10.1088/1361-6579/acdcdd.
- [25] David E. Haines, Denny D. Watson, Tissue Heating During Radiofrequency Catheter Ablation: a Thermodynamic Model and Observations in Isolated Perfused and Superfused Canine Right Ventricular Free Wall, Pacing. Clin. Electrophysiol. 12 (6) (1989) 962–976, https://doi.org/10.1111/j.1540-8159.1989.tb05034.x.
- [26] J.G. Whayne, S. Nath, D.E. Haines, Microwave Catheter Ablation of Myocardium in Vitro. Assessment of the Characteristics of Tissue Heating and Injury, Circulation 89 (5) (1994) 2390–2395, https://doi.org/10.1161/01.CIR.89.5.2390.